RECLAMATION

Managing Water in the West

Report DSO-07-04

The Incident Wave Method for Incorporating Earthquake Excitation in Finite Element Analyses

Dam Safety Technology Development Program

U.S. Department of the Interior
Bureau of Reclamation
Technical Service Center
Denver, Colorado

August 2005

DRAFT 8/28/05

THE INCIDENT WAVE METHOD FOR INCORPORATING EARTHQUAKE EXCITATION IN FINITE ELEMENT ANALYSES

John F. Hall
California Institute of Technology

INTRODUCTION

This paper is concerned with incorporating earthquake excitation in the analysis of a structure using methods that allow for interaction between the structure and its supporting region (soil, rock, etc.), include spatial nonlinearity in the excitation, and permit the structure and some of the adjacent supporting region to undergo nonlinear behavior. This is the most general case. Two techniques are discussed: a three-step, free-field method and a simpler incident wave method. The main purpose of this paper is to reveal some previously unrecognized problems with the incident wave method. These problems do not arise with the free-field method. A corrected incident wave method is also discussed. For background information, the reader is directed to an extensive literature (…..).

FREE-FIELD METHOD

The system to be analyzed is divided into two parts denoted 1 and 2. Part 1 contains the entire structure and the part of the supporting region that exhibits nonlinear behavior. Part 2 consists of the rest of the supporting region, which is assumed to remain linearly elastic. These features are illustrated in Figure 1 where Part 1 includes the dam and water (together considered to be the structure) and some of the adjacent supporting region.

The free-field method consists of three steps. First is computation of the free-field motions, defined as the motions that the earthquake would produce at the interface between Parts 1 and 2 if Part 1 were absent. As far as Part 1 is concerned, these free-field motions completely define the earthquake, and they can be constructed empirically, analytically or by some numerical method. This process may be made easier if the interface between Parts 1 and 2 is located to simplify the geometries involved. Relocation of this interface is possible by placing any amount of the linearly elastic portion of the supporting region into Part 1. Details of computing the free-field motions are not presented here.

The second step is to find a set of forces that, when applied to Part 2 with Part 1 removed, causes the interface between Part 2 and the absent Part 1 to move at the free-field motions obtained in the first step. For this purpose, consider a truncated Part 2

where the infinite extent has been replaced by transmitting boundaries (Figure 2). A finite element discretization is employed to obtain the equations of motion of Part 2 as

$$\begin{bmatrix} \overline{K}_{ii} & \overline{K}_{i2} \\ \overline{K}_{i2}^T & \overline{K}_{22} \end{bmatrix} \begin{Bmatrix} d_i(t) \\ d_2(t) \end{Bmatrix} + \begin{bmatrix} \overline{C}_{ii} & \overline{C}_{i2} \\ \overline{C}_{i2}^T & \overline{C}_{22} \end{bmatrix} \begin{Bmatrix} v_i(t) \\ v_2(t) \end{Bmatrix} + \begin{bmatrix} \overline{M}_{ii} & \overline{M}_{i2} \\ \overline{M}_{i2}^T & \overline{M}_{22} \end{bmatrix} \begin{Bmatrix} a_i(t) \\ a_2(t) \end{Bmatrix} = \begin{Bmatrix} f_i(t) \\ f_2(t) \end{Bmatrix} \qquad (1)$$

where $[\overline{K}]$, $[\overline{C}]$ and $[\overline{M}]$ are stiffness, damping and mass matrices, which include appropriate transmitting boundary terms; the overbar denotes that these matrices are computed from the finite element discretization of Part 2; $\{d(t)\}$, $\{v(t)\}$ and $\{a(t)\}$ are displacement, velocity and acceleration degree-of-freedom vectors; (t) denotes function of time; *i* denotes the degrees of freedom on the interface with the absent Part 1; the 2 denotes the degrees of freedom of Part 2 not located on the interface; and $\{f(t)\}$ is the dynamic load vector. To compute the forces to be applied to Part 2 to represent the earthquake, insert the free-field motions from the first step for the interface degrees of freedom and insert any arbitrary motion for the other degrees of freedom; thus,

$$\begin{Bmatrix} f_i^{eq}(t) \\ f_2^{eq}(t) \end{Bmatrix} = \begin{bmatrix} \overline{K}_{ii} & \overline{K}_{i2} \\ \overline{K}_{i2}^T & \overline{K}_{22} \end{bmatrix} \begin{Bmatrix} d_i^{ff}(t) \\ d_2^{arb}(t) \end{Bmatrix} + \begin{bmatrix} \overline{C}_{ii} & \overline{C}_{i2} \\ \overline{C}_{i2}^T & \overline{C}_{22} \end{bmatrix} \begin{Bmatrix} v_i^{ff}(t) \\ v_2^{arb}(t) \end{Bmatrix} + \begin{bmatrix} \overline{M}_{ii} & \overline{M}_{i2} \\ \overline{M}_{i2}^T & \overline{M}_{22} \end{bmatrix} \begin{Bmatrix} a_i^{ff}(t) \\ a_2^{arb}(t) \end{Bmatrix} \qquad (2)$$

where *eq* signifies that the forces generate the earthquake; *ff* denotes the free-field motions; and *arb* denotes the arbitrary motions. Choice of the arbitrary motions, which could even be taken as zero, should not affect the final result except possibly for some numerical accuracy issues. This is not discussed here except to say that equation (1) should be solved with the loads from equation (2) to ensure that the resulting motions of the interface degrees of freedom are close to the desired free-field displacements, velocities and accelerations.

The final step is to apply the earthquake loads to a combined finite element discretization of Parts 1 and 2, which entails solving

$$\begin{Bmatrix} R_1(t) \\ R_i(t) \\ 0 \end{Bmatrix} + \begin{bmatrix} 0 & 0 & 0 \\ 0 & \overline{K}_{ii} & \overline{K}_{i2} \\ 0 & \overline{K}_{i2}^T & \overline{K}_{22} \end{bmatrix} \begin{Bmatrix} d_1(t) \\ d_i(t) \\ d_2(t) \end{Bmatrix} + \begin{bmatrix} C_{11} & C_{1i} & 0 \\ C_{1i}^T & C_{ii} + \overline{C}_{ii} & \overline{C}_{i2} \\ 0 & \overline{C}_{i2}^T & \overline{C}_{22} \end{bmatrix} \begin{Bmatrix} v_1(t) \\ v_i(t) \\ v_2(t) \end{Bmatrix} +$$
$$\begin{bmatrix} M_{11} & M_{1i} & 0 \\ M_{1i}^T & M_{ii} + \overline{M}_{ii} & \overline{M}_{i2} \\ 0 & \overline{M}_{i2}^T & \overline{M}_{22} \end{bmatrix} \begin{Bmatrix} a_1(t) \\ a_i(t) \\ a_2(t) \end{Bmatrix} = \begin{Bmatrix} f_1^{st} \\ f_i^{st} + f_i^{eq}(t) \\ f_2^{st} + f_2^{eq}(t) \end{Bmatrix} \qquad (3)$$

where $\{R(t)\}$ is the vector of nonlinear stiffness forces for Part 1; $[C]$ and $[M]$ are damping and stiffness matrices for Part 1; the 1 denotes the degrees of freedom of Part 1 not located on the interface with Part 2; and $\{f^{st}\}$ is the static load vector. Equation (3)

can be solved by standard methods consisting of a static solution for the static loads and a dynamic analysis for the earthquake loads (ref).

In equation (3), nonlinear effects have been assumed to be associated only with the Part 1 stiffness. Motions computed from equation (3) are total motions for the types 1 and *i* degrees of freedom, but not for the type 2 degrees of freedom. This is why Part 2 must remain linearly elastic, i.e., superposition would be necessary to obtain the total motions of the Part 2 degrees of freedom.

INCIDENT WAVE METHOD

The earthquake is represented by incident waves that propagate in the supporting region toward the structure. With reference to Figure 3, a common technique is to generate upward propagating S and P waves by applying tractions to the base of the supporting region, where the bottom transmitting boundary is also located. In Figure 3, *x* and *y* are horizontal coordinates and *z* is vertical. According to 1-dimensional wave propagation theory, uniformly distributed *x* and *y* tractions can be used to generate planar S_x and S_y waves, respectively, and uniformly distributed *z* tractions can be used to generate planar *P* waves. These tractions must generate the incident waves as well as move the transmitting boundary. Thus, they consist of two parts, which can be computed separately.

Let $d_{x,inc}(t)$, $v_{x,inc}(t)$ and $a_{x,inc}(t)$ denote the *x* components of the displacement, velocity and acceleration of the incident wave as generated at the base of the supporting region, similarly for the *y* and *z* components. For a linearly elastic, homogeneous supporting region, this incident motion can be simply taken as one half any desired reference motion at the top surface, because of the doubling effect when a wave reaches a free surface. For a nonhomogeneous region where the material properties are a function only of the *z* coordinate, a deconvolution can be performed to determine the appropriate incident wave form. Based on 1-dimensional wave propagation theory and considering first the case where the transmitting boundary (t.b.) at the base is not present, the tractions applied to the bottom surface of the supporting region to produce the desired incident wave motion are

$$t_x^{eq}(t) = \frac{G}{C_S} v_{x,inc}(t);\ \ t_y^{eq}(t) = \frac{G}{C_S} v_{y,inc}(t);\ \ t_z^{eq}(t) = \frac{E'}{C_P} v_{z,inc}(t) \quad \text{(4, no bottom t.b.)}$$

where *eq* signifies that the tractions generate the incident waves representing the earthquake; *G* is the shear modulus; $E' = E(1-\nu)/(1-\nu-2\nu^2)$; *E* is Young's modulus, ν is Poisson's ratio; C_S is the S wave speed; and C_P is the *P* wave speed. In equation (4), $t_x^{eq}(t)$ and $t_y^{eq}(t)$ are shear tractions and $t_z^{eq}(t)$ is a normal traction.

A simple and commonly used transmitting boundary, which is also based on 1-dimensinal wave propagation theory, applies tractions to the base of the supporting region proportional to and with opposite sign to the velocity there (ref):

$$t_x^{tb}(t) = -\frac{G}{C_S} v_x(t);\ \ t_y^{tb}(t) = -\frac{G}{C_S} v_y(t);\ \ t_z^{tb}(t) = -\frac{E'}{C_P} v_z(t) \quad (5)$$

where *tb* denotes tractions applied by the transmitting boundary. Therefore, when this transmitting boundary is present at the base of the supporting region, additional tractions in the amount given by equation (4) must be applied to move the base at the incident wave motions. Thus, the tractions from equation (4) must be doubled:

$$t_x^{eq}(t) = 2\frac{G}{C_S} v_{x,inc}(t);\ \ t_y^{eq}(t) = 2\frac{G}{C_S} v_{y,inc}(t);\ \ t_z^{eq}(t) = 2\frac{E'}{C_P} v_{z,inc}(t). \quad \text{(6, with bottom t.b.)}$$

This doubling is reasonable since these tractions are essentially generating both upward and downward propagating waves, hence, the factor of two.

In the finite element discretization, the tractions from equation (6) are converted to nodal forces $\{f^{eq}(t)\}$ in the usual way. The equation of motion to be solved is

$$\{R(t)\} + [C]\{v(t)\} + [M]\{a(t)\} = \{f^{st}\} + \{f^{eq}(t)\} \quad (7)$$

where the nodal forces in $\{f^{eq}(t)\}$ are non-zero for only degrees of freedom at the nodes on the bottom of the supporting region. The transmitting boundary condition given by equation (5), as well as similar conditions along the sides of the supporting region adjusted for different normal and tangent directions, are incorporated into the damping matrix $[C]$. More exact transmitting boundaries could also be used. In general, transmitting boundaries only replace regions that remain linearly elastic; however, both the structure and the supporting region shown in Figure 3 can be nonlinear.

FREQUENCY-DOMAIN TEST OF THE INCIDENT WAVE METHOD

The intent of the incident wave method is to generate planar S_x, S_y and P waves at the base of the supporting region that will then travel upward toward the structure. After generation, the 1-dimensional character of the wave propagation will be appropriately modified by inhomogeneity in the medium, irregular surface features, the presence of the structure to be analyzed, and any nonlinear behavior. However, the transmitting boundaries along the sides of the supporting region, which are designed to absorb outward propagating waves generated by the aforementioned factors, are not compatible with the upward traveling incident waves. This can alter the desired motions imparted to the structure, and the effect can be surprisingly large.

To investigate, consider a test problem consisting of a rectangular block of depth *h* and lateral dimensions 2*h* by 2*h*. The material is linearly elastic and homogeneous, and Poisson's ratio is taken as 0.20. Symmetry considerations allow only one quarter of the block to be modeled (Figure 4). The analysis is performed in the frequency domain with normalized frequency parameter

$$\tilde{\omega} = \omega \frac{h}{C_S} \qquad (8)$$

where ω is the actual frequency in *rad/s*. Thus, in a normalized time of one, a shear wave travels the block depth *h*. Spatially uniform tractions $t_x^{eq}(\tilde{\omega})$ and $t_z^{eq}(\tilde{\omega})$ are applied to the base of the block, and response velocities are computed.

When $t_x^{eq}(\tilde{\omega})$ is applied, the velocity components are normalized as

$$\tilde{v}_x(\tilde{\omega}) = v_x(\tilde{\omega}) \frac{1}{t_x^{eq}(\tilde{\omega})} \frac{G}{C_S}; \;\; \tilde{v}_y(\tilde{\omega}) = v_y(\tilde{\omega}) \frac{1}{t_x^{eq}(\tilde{\omega})} \frac{G}{C_S}; \;\; \tilde{v}_z(\tilde{\omega}) = v_z(\tilde{\omega}) \frac{1}{t_x^{eq}(\tilde{\omega})} \frac{G}{C_S} \qquad (9)$$

where $v_x(\tilde{\omega})$, $v_y(\tilde{\omega})$ and $v_z(\tilde{\omega})$ are the components of the actual velocity, and $t_x^{eq}(\tilde{\omega})$ is taken from the frequency-domain version of equation 6 with $v_{x,inc}(\tilde{\omega})$ equal to one half. Under conditions of 1-dimensional wave propagation in an infinite medium, the generated incident S_x wave will cause velocity amplitudes at the top surface of $\tilde{v}_x(\tilde{\omega}) = 1, \tilde{v}_y(\tilde{\omega}) = 0,$ and $\tilde{v}_z(\tilde{\omega}) = 0$. For this test problem under application of $t_x^{eq}(\tilde{\omega})$, this is the desired motion. When $t_z^{eq}(\tilde{\omega})$ is applied, the velocity components are normalized as

$$\tilde{v}_x(\tilde{\omega}) = v_x(\tilde{\omega}) \frac{1}{t_z^{eq}(\tilde{\omega})} \frac{E'}{C_P}; \;\; \tilde{v}_y(\tilde{\omega}) = v_y(\tilde{\omega}) \frac{1}{t_z^{eq}(\tilde{\omega})} \frac{E'}{C_P}; \;\; \tilde{v}_z(\tilde{\omega}) = v_z(\tilde{\omega}) \frac{1}{t_z^{eq}(\tilde{\omega})} \frac{E'}{C_P}, \qquad (10)$$

where $t_z^{eq}(\tilde{\omega})$ is taken from the frequency-domain version of equation 6 with $v_{z,inc}(\tilde{\omega})$ equal to one half. Under conditions of 1-dimensional wave propagation in an infinite medium, the generated incident *P* wave will cause velocity amplitudes at the top surface of $\tilde{v}_x(\tilde{\omega}) = 0, \tilde{v}_y(\tilde{\omega}) = 0,$ and $\tilde{v}_z(\tilde{\omega}) = 1$. For this test problem under application of $t_z^{eq}(\tilde{\omega})$, this is the desired motion.

In the finite element discretization, cubic 8-noded solid elements are employed with side length *h*/16. Thus, a total of 4096 elements are needed for the quarter block shown in Figure 4. In some of the results, mass-proportional damping is added over the domain of the block in the amount of 5% of critical at a normalized frequency of $\tilde{\omega} = 1.6 \cdot \pi$ *rad/s*.

Two types of results are presented. First is the amplitude of the complex-valued frequency response function for normalized velocity at point C, the center point of the top surface of the full block, as a function of normalized frequency from $\tilde{\omega} = 0$ to $\tilde{\omega} = 8 \cdot \pi$ (Figures 5 to 8). Components $\tilde{v}_x(\tilde{\omega})$ and $\tilde{v}_z(\tilde{\omega})$ at point C are plotted when $t_x^{eq}(\tilde{\omega})$ and $t_z^{eq}(\tilde{\omega})$ are applied, respectively. Frequency responses are presented for three cases of boundary conditions on the two exterior sides of the quarter block at $x = h$ and $y = h$: conditions to force a 1-dimensional wave propagation solution (Case 1D), traction-free conditions (Case F), and the transmitting boundary conditions (Case TB). For Case TB, the equations used in the transmitting boundary are the frequency-domain versions of

$$t_x^{tb}(t) = -\frac{E'}{C_P} v_x(t); \;\; t_y^{tb}(t) = -\frac{G}{C_S} v_y(t); \;\; t_z^{tb}(t) = -\frac{G}{C_S} v_z(t) \qquad (11)$$

on side $x = h$ and

$$t_x^{tb}(t) = -\frac{G}{C_S} v_x(t); \;\; t_y^{tb}(t) = -\frac{E'}{C_P} v_y(t); \;\; t_z^{tb}(t) = -\frac{G}{C_S} v_z(t) \qquad (12)$$

on side $y = h$. For all three cases, the transmitting boundary condition of equation (5) is used at the base of the supporting region.

The second type of result shows the normalized velocity response shapes of three faces of the quarter block at selected frequencies for Case TB where transmitting boundaries are used on the exterior sides. The three faces over which the response shapes are shown are the $y = 0$ plane of symmetry viewed from a negative *y* position, the $x = 0$ plane of symmetry viewed from a positive *x* position, and the top face at $z = h$ viewed from above. At each frequency, a group of six plots is presented. The top row of three plots are the normalized velocity shapes of the three faces at the instant of time when a component of velocity of point C ($\tilde{v}_x(\tilde{\omega})$ when $t_x(\tilde{\omega})$ is applied, $\tilde{v}_z(\tilde{\omega})$ when $t_z(\tilde{\omega})$ is applied) reaches its maximum value. The bottom row of three plots reveals phase information, showing normalized velocity shapes at the instant of time when the aforementioned velocity components reach zero. All six plots in each group are plotted to the same scale; a normalized velocity amplitude of one extends over two undeformed element lengths. An undeformed mesh appears shaded in the background for reference. A key diagram is provided in Figure 9, and the velocity response shapes are shown in Figures 10 and 11 for application of $t_x^{eq}(\tilde{\omega})$ and $t_z^{eq}(\tilde{\omega})$, respectively.

Results for application of $t_x^{eq}(\tilde{\omega})$. The desired response of the block is 1-dimensional where the top surface moves uniformly in the *x* direction at a frequency-independent normalized velocity of one. Case 1D achieves this 1-dimensional response by fixing the *z* degrees of freedom on the exterior face $x = h$. As shown in Figure 5, the amplitude of the normalized velocity $\tilde{v}_x(\tilde{\omega})$ is correct at $\tilde{\omega} = 0$. At this zero frequency the block

moves as an unstressed rigid body. However, frequency independence is not achieved as peaks in the normalized velocity occur at the frequencies of the discretized block's fixed-base shear modes, which, for the lower modes, are approximately equal to the normalized frequencies of the continuous block given by

$$\tilde{\omega}_i = \frac{\pi}{2}(2i-1);\ i = 1,2,3\ldots \qquad (13)$$

The peaks in Figure 5, whose heights increase with frequency, are due to reflections off the bottom surface of the block where the transmitting boundary is located. The transmitting boundary is not exact when used with a finite element discretization of the block, even for this 1-dimensional response where the waves are plane and normally incident. This effect can be reduced by refining the finite element mesh in the vertical direction.

Also shown in Figure 5 is the normalized velocity $\tilde{v}_x(\tilde{\omega})$ at point C when the exterior faces $x = h$ and $y = h$ are treated as free surfaces (Case F). Compared to Case 1D, this just involves freeing the *z* degrees of freedom at the $x = h$ face, which does not alter the response of the block at $\tilde{\omega} = 0$ since the motion is stress free. However, there is a dramatic effect at higher frequencies where a pronounced frequency independence is introduced due to many 3-dimensinal modes being excited. Peak amplitudes exceed twice the desired response amplitude of one.

Results for normalized velocity $\tilde{v}_x(\tilde{\omega})$ at point C when transmitting boundaries are employed on the exterior faces $x = h$ and $y = h$ (Case TB) are presented in Figure 6. At $\tilde{\omega} = 0$ a drag effect from the side transmitting boundaries as well as a rotational component of the block motion reduces $\tilde{v}_x(\tilde{\omega})$ at point C to a value of 0.17, much less than the desired value of one. At higher frequencies, the response exhibits considerable variation with frequency, although less than that of Case F because of the extra damping effect of the side transmitting boundaries. Across the frequency range considered, the average response amplitude is close to one, although the fluctuations exceed 50% of the average amplitude. When mass-proportional damping is added, the frequency variations are suppressed further, and the average level of response drops to about 0.70 over the frequency range considered.

Response shapes of the block for normalized velocity at the four frequencies marked in Figure 6 are shown in Figure 10 for Case TB without mass-proportional damping. Certainly, the block does not respond under 1-dimensional wave propagation as intended; the deformations are very 3-dimensional. In addition to the false frequency variations that are introduced into the motion of the top surface, where a structure would be located, there is false spatial nonuniformity as well. These spatial variations could be significant in the case of an extended structure, such as a bridge. The exterior faces $x = h$ and $y = h$ containing the side transmitting boundaries are more restrained in their motion compared to the rest of the block.

Results for application of $t_z^{eq}(\tilde{\omega})$. The desired response of the block is 1-dimensional where the top surface moves uniformly in the *z* direction at a frequency-independent normalized velocity of one. Case 1D achieves this 1-dimensional response by fixing the *x* degrees of freedom on the exterior face $x = h$ and the *y* degrees of freedom on the exterior face $y = h$. As shown in Figure 7, the amplitude of the normalized velocity $\tilde{v}_z(\tilde{\omega})$ is correct at $\tilde{\omega} = 0$. At this zero frequency the block moves as an unstressed rigid body. However, frequency independence is not achieved as peaks in the normalized velocity occur at the frequencies of the discretized block's fixed-base vertical modes, which, for the lower modes, are approximately equal to the normalized frequencies of the continuous block given by

$$\tilde{\omega}_i = \frac{\pi}{2}(2i-1)\frac{C_P}{C_S};\ i = 1,2,3\ldots \qquad (13)$$

with peak height increasing with frequency. The effect is similar to that observed for Case 1D involving application of $t_x^{eq}(\tilde{\omega})$, and can also be reduced by refining the finite element mesh in the vertical direction.

Also shown in Figure 7 is the normalized velocity $\tilde{v}_z(\tilde{\omega})$ at point C when the exterior faces $x = h$ and $y = h$ are treated as free surfaces (Case F). Compared to Case 1D, this just involves freeing the degrees of freedom in these faces' respective normal directions, which does not alter the response of the block at $\tilde{\omega} = 0$ since the motion is stress free. However, a pronounced frequency independence is introduced at higher frequencies due to many 3-dimensinal modes being excited. Peak amplitudes exceed twice the desired response amplitude of one. This effect is similar to that seen for Case F involving application of $t_x^{eq}(\tilde{\omega})$; although, in the present case the large frequency variations can be attributed entirely to Poisson's ratio being non-zero. If Poisson's ratio were zero, no lateral strains occur, and the response becomes 1-dimensional.

Results for normalized velocity $\tilde{v}_z(\tilde{\omega})$ at point C when transmitting boundaries are employed on the exterior faces $x = h$ and $y = h$ (Case TB) are presented in Figure 8. At $\tilde{\omega} = 0$ a drag effect from the side transmitting boundaries reduces $\tilde{v}_z(\tilde{\omega})$ at point C below one to a value of 0.45. At higher frequencies, the response exhibits considerable variation with frequency, although less than that of Case F because of the extra damping effect of the side transmitting boundaries. Across the frequency range considered, the average response amplitude is close to one although the fluctuations exceed 50% of the average amplitude. Addition of mass-proportional damping further suppresses the frequency variations and reduces the average level of response to about 0.85 over the frequency range considered.

Response shapes of the block for normalized velocity at the six frequencies marked in Figure 8 are shown in Figure 11 for Case TB without mass-proportional

damping. The deformation is very 3-dimensional, not at all 1-dimensional as intended. The motion of the top surface exhibits significant false frequency variations as well as false spatial nonuniformity. The transmitting boundaries on the exterior faces $x = h$ and $y = h$ restrain the motion of these faces compared to the rest of the block.

TIME-DOMAIN TEST OF THE INCIDENT WAVE METHOD

The same system from the previous section is employed except that the response of the block is computed in the time domain. Only Case TB without mass-proportional damping is examined. The ratio h / C_S is selected as 0.25 *s*, which means that the maximum actual frequency in the plots of Figures 5 to 8 is $\omega = 32 \cdot \pi$ *rad/s*. The desired motion for the block's top surface is selected as a horizontal component from the Olive View Hospital free-field site during the 1994 Northridge earthquake. Displacement, velocity and acceleration time histories are shown on the left side of Figure 12, along with 5% damped displacement and pseudo-acceleration response spectra on the left side of Figure 13. For use as the incident velocity $v_{x,inc}(t)$ in equation (6) to compute $t_x^{eq}(t)$, the Olive View Hospital time history is halved in amplitude because of the doubling that occurs during reflection at the top surface of the block. Only $t_x^{eq}(t)$ is applied.

The resulting motions at point C in the *x* direction are shown on the right side of Figure 12. These are computed by direct time integration of the finite element equations of motion. Also shown are the 5% damped displacement and pseudo-acceleration response spectra on the right side of Figure 13. The significant differences between the computed results on the right and the desired results on the left are consistent with the differences between the frequency-domain response shown in Figure 6 without mass-proportional damping and the desired response amplitude of one for the normalized velocity. Computed peak values of displacement, velocity and acceleration at point C in the *x* direction are -8.3 *cm*, -38 *cm/s* and 598 cm/s^2 compared to the desired peak values of -31.3 *cm*, -131 *cm/s* and 818 cm/s^2, respectively.

IMPROVED INCIDENT WAVE METHOD

As demonstrated in the previous two sections with the rectangular block test problem, the motions generated by the incident wave method are adversely affected by the presence of transmitting boundaries on the sides of the block and by the excitation of 3-dimensional modes of the block. False frequency and spatial variations are both introduced. Of interest is how the incident wave method can be corrected, other than just using the alternative free-field method. One technique would be to extend the lateral dimensions of the supporting region; however, this is not likely to be computationally efficient. Another technique involves modifying the earthquake force vector $\{f^{eq}(t)\}$ in equation (7) as described below, although there are certain limitations. Included in the discussion is a more detailed explanation than given previously of how the incident wave motions are derived.

Consider a rectangular block of dimensions $l \times w \times h$ such as shown in Figure 4, where material properties vary only in the vertical direction. The material profile should match as closely as possible that of the site where the structure to be analyzed is located. The set of forces $\{f^{eq}(t)\}$ representing the earthquake is constructed using a finite element discretization of this block with transmitting boundaries on the sides and bottom. The earthquake itself is defined by specifying the time histories of upwardly incident, planar S_x, S_y and P waves at the bottom surface of the block in terms of $v_{x,inc}(t)$, $v_{y,inc}(t)$ and $v_{z,inc}(t)$ in equation (6). These wave time histories can be computed using a 1-dimensional deconvolution applied to a selected earthquake record appropriate in terms of event magnitude and distance to the fault. With reference to Figure 14, suppose the chosen record is from a site where the material profile is a-b-c-d, which could be different in its upper part from the profile a'-b'-b-c-d where the structure to be analyzed is located. The deconvolution is performed using the profile a-b-c to obtain the incident motions at the bottom of the block.

The forces $\{f^{eq}(t)\}$ are comprised of several contributions. First are the nodal forces $\{f_1^{eq}(t)\}$ corresponding to tractions given by equation (6). These are the same forces used in the incident wave method described previously and consist of two parts: one to generate the upward propagating S_x, S_y and P waves and the other to move the transmitting boundary at the bottom of the block. The material properties E, G and ν in equation (6) are the values at the bottom of the block.

In the improved method, additional contributions $\{f_2^{eq}(t)\}$ and $\{f_3^{eq}(t)\}$ are needed along the sides of the block to ensure that the block undergoes a 1-dimensional response for each wave type. The S_x and S_y wave parts of the response require nodal forces on the sides of the block in the z degrees of freedom to keep them from moving. The P wave part of the response requires nodal forces on the $x = \pm d/2$ sides in the x degrees of freedom and on the $y = \pm w/2$ sides in the y degrees of freedom to keep these two sets of degrees of freedom from moving. The nodal forces $\{f_2^{eq}(t)\}$ can be computed from two dynamic analyses in which the S_x and S_y parts of $\{f_1^{eq}(t)\}$ are applied in one and the P wave part of $\{f_1^{eq}(t)\}$ is applied in the other. Fixity conditions are employed for all degrees of freedom to be held motionless, and $\{f_2^{eq}(t)\}$ is constructed from both sets of reaction forces. In these analyses, the transmitting boundaries on the sides of the block are omitted. However, since these transmitting boundaries should actually be present, additional nodal forces $\{f_3^{eq}(t)\}$ are needed to move the sides of the block at the computed x and y motions for the S_x/S_y wave analysis and at the computed z motions for the P wave analysis. The forces $\{f_3^{eq}(t)\}$ are found by multiplying these computed motions by corresponding transmitting boundary terms.

The force vector $\{f^{eq}(t)\}$ is then

$$\left\{f^{eq}(t)\right\} = \left\{f_1^{eq}(t)\right\} + \left\{f_2^{eq}(t)\right\} + \left\{f_3^{eq}(t)\right\}. \qquad (14)$$

When $\left\{f^{eq}(t)\right\}$ is applied to the block with all transmitting boundaries present, the block responds in planar S_x, S_y and P waves propagating vertically (up and down), each wave being a 1-dimensional response of the block. A requirement is that this solution be linearly elastic.

With the earthquake represented by $\left\{f^{eq}(t)\right\}$, these forces can be applied to a modified block that contains the structure to be analyzed, local topography, and local variations in material properties. Behavior within the modified block can be nonlinear. The only restriction on the modifications is that the geometry and finite element discretization on the sides and bottom of the block, where the forces $\left\{f^{eq}(t)\right\}$ are applied, can not be altered. These features constitute the improved incident wave method. The errors quantified in Figures 5 to 13 for the original incident wave method are the results of omitting the forces $\left\{f_2^{eq}(t)\right\}$ and $\left\{f_3^{eq}(t)\right\}$ from the analyses.

CONCLUSIONS

The incident wave method as commonly applied may involve errors in the earthquake motions incident to a structure due to the excitation of 3-dimensinal modes of the supporting region and due to an effect of the transmitting boundaries on the sides of this region. These errors can be quite significant, as demonstrated in this paper on a test problem consisting of a simple rectangular block. To avoid the problem, the incident wave method can be corrected with additional forces on the sides of the supporting region. An alternative free-field method can also be employed.

REFERENCES

1.

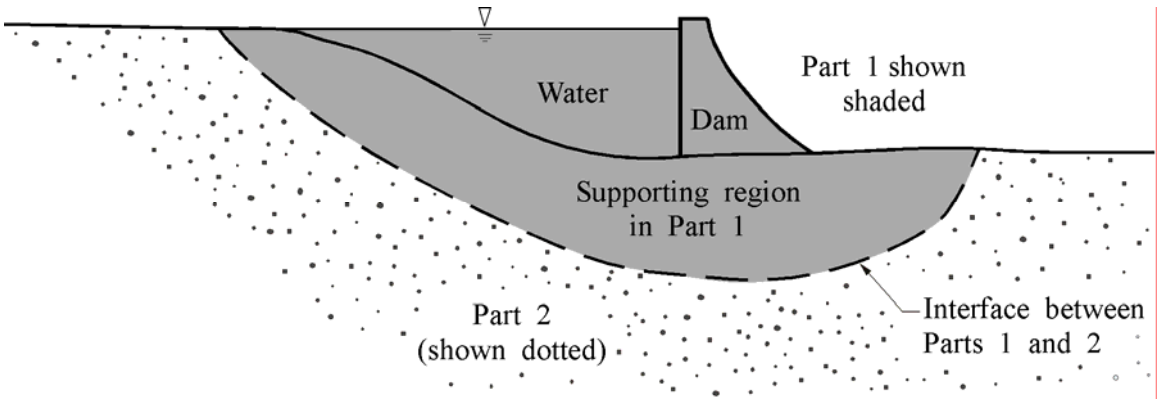

Figure 1. Division of the system to be analyzed by the free-field method into Part 1, consisting of the structure (dam and water) and the portion of the supporting region that exhibits nonlinear behavior, and Part 2, consisting of the rest of the supporting region.

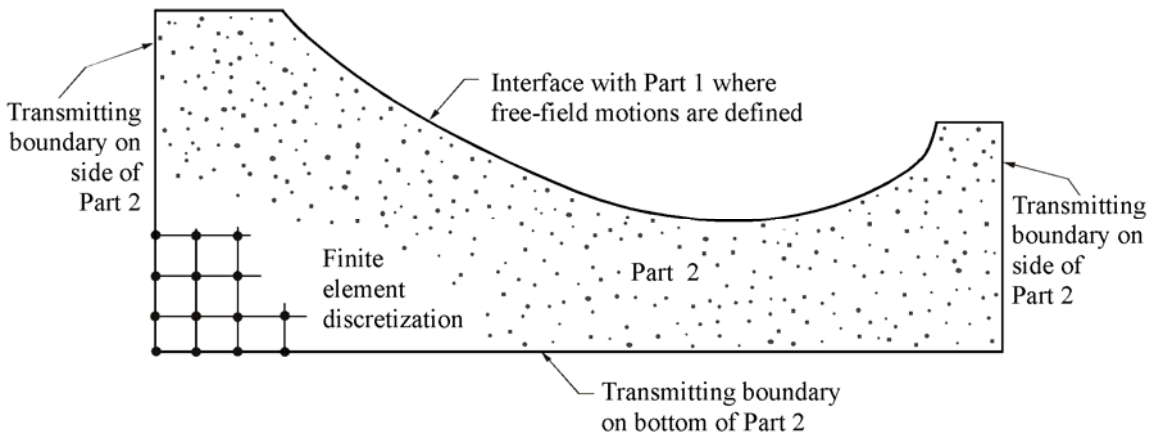

Figure 2. Part 2 of the system to be analyzed by the free-field method, used with Part 1 absent to compute the forces that represent the earthquake. Infinite extent of Part 2 has been replaced by transmitting boundaries.

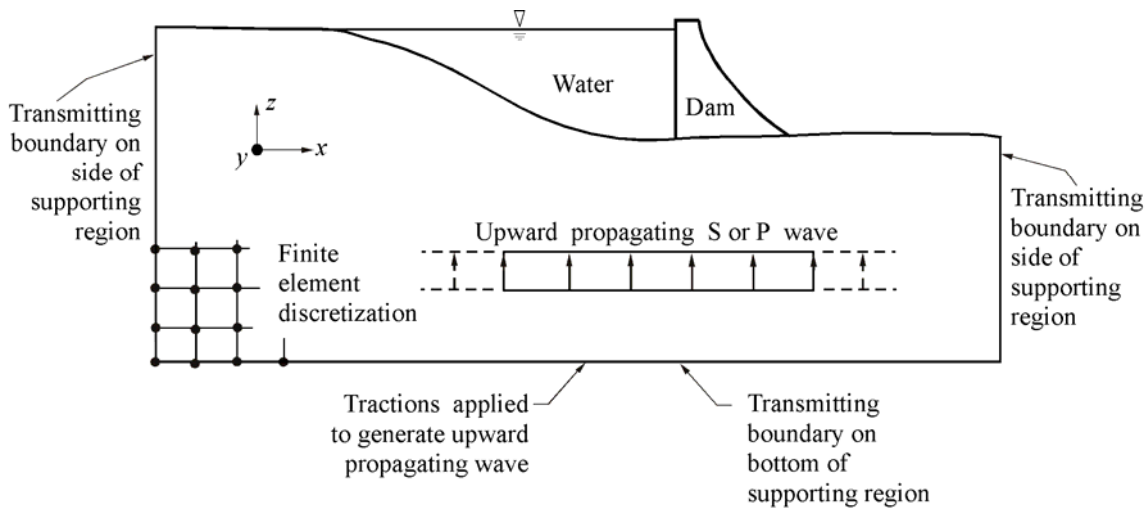

Figure 3. System to be analyzed by the incident wave method showing earthquake waves generated by tractions applied to bottom of the supporting region.

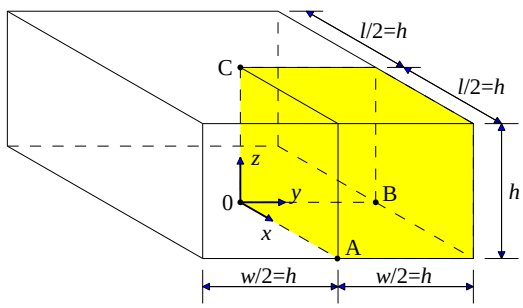

Figure 4. Quarter foundation block (shown shaded) used in test problem of the incident wave method.

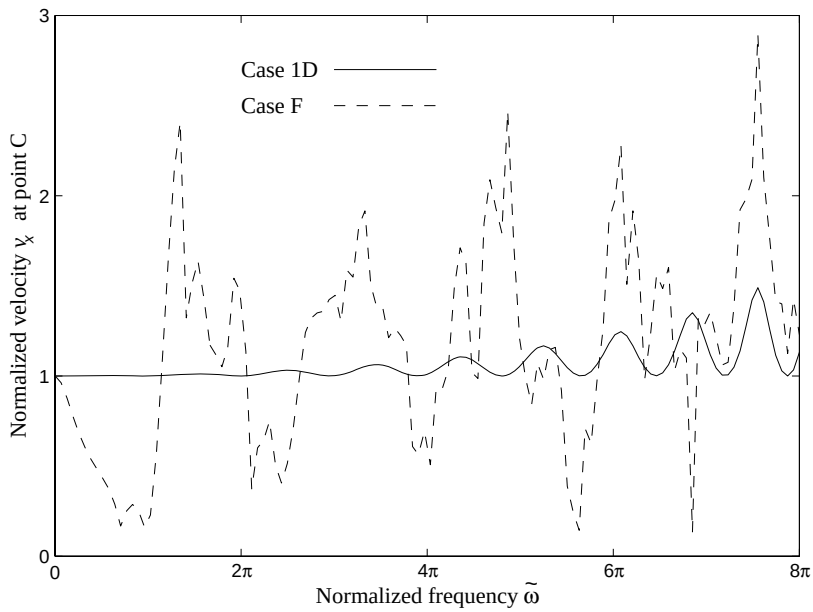

Figure 5. Frequency response of the normalized velocity $\tilde{v}_x(\tilde{\omega})$ at point C for application of $t_x^{eq}(\tilde{\omega})$. Cases 1D and F.

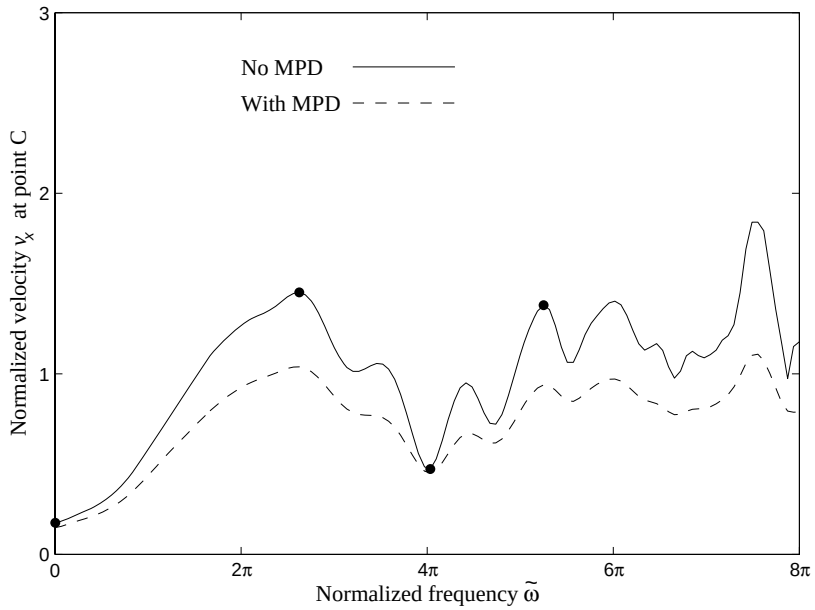

Figure 6. Frequency response of the normalized velocity $\tilde{v}_x(\tilde{\omega})$ at point C for application of $t_x^{eq}(\tilde{\omega})$. Case TB without mass-proportional damping (MPD). Dots denote where response shapes are plotted in Figure 10.

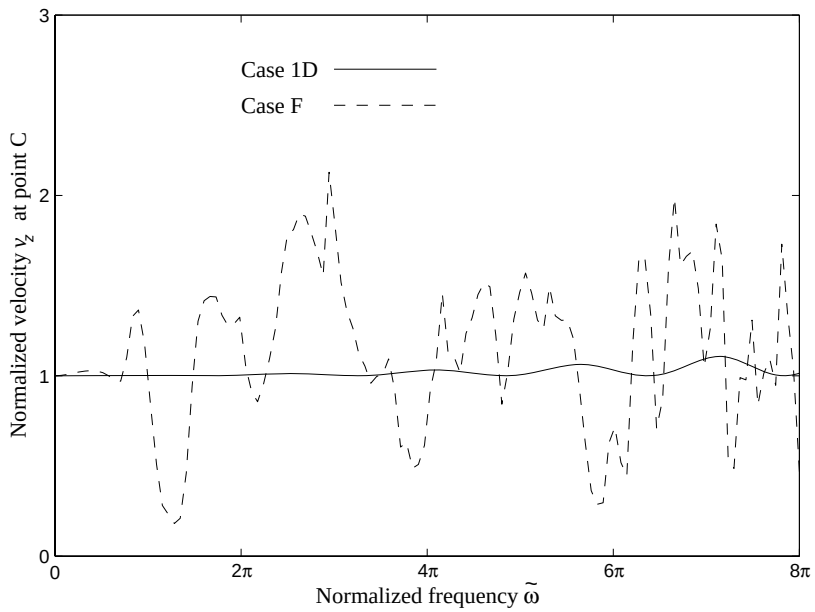

Figure 7. Frequency response of the normalized velocity $\tilde{v}_z(\tilde{\omega})$ at point C for application of $t_z^{eq}(\tilde{\omega})$. Cases 1D and F.

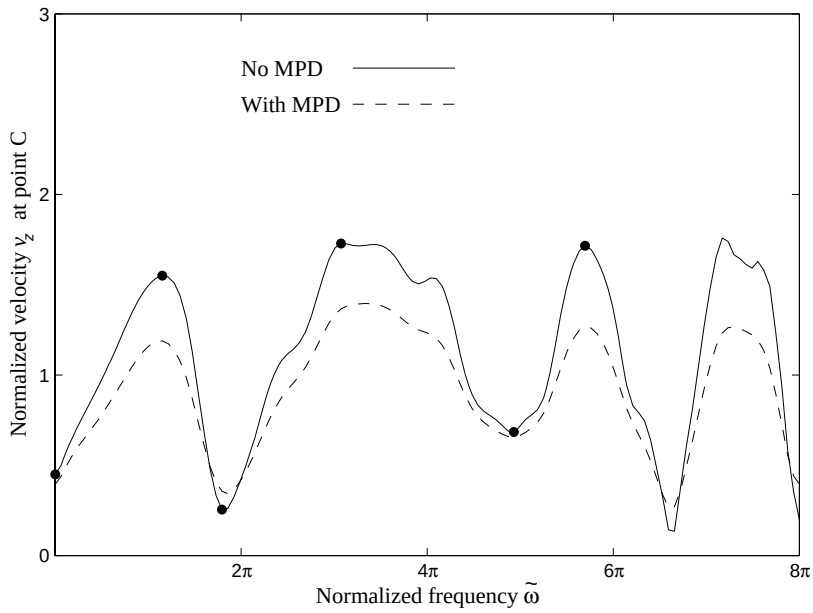

Figure 8. Frequency response of the normalized velocity $\tilde{v}_z(\tilde{\omega})$ at point C for application of $t_z^{eq}(\tilde{\omega})$. Case TB without mass-proportional damping (MPD). Dots denote where response shapes are plotted in Figure 11.

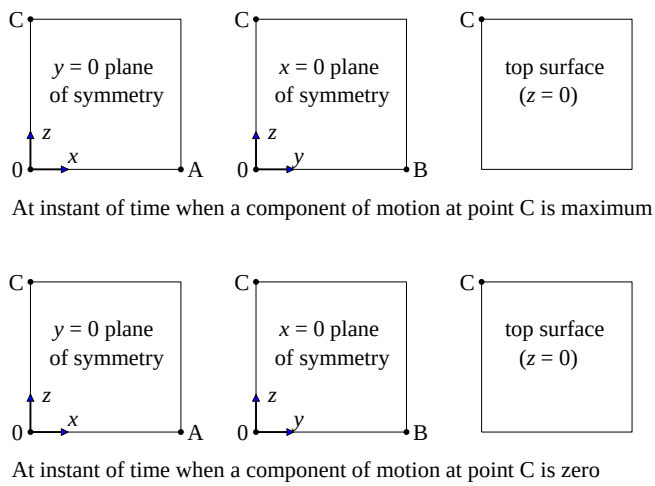

Figure 9. Key diagram for plots of normalized velocity response shapes at selected frequencies; plots are shown in Figure 10 (t_x^{eq} applied) and Figure 11 (t_z^{eq} applied). Component of motion referred to in this figure is *x* when t_x^{eq} is applied and *z* when t_z^{eq} is applied.

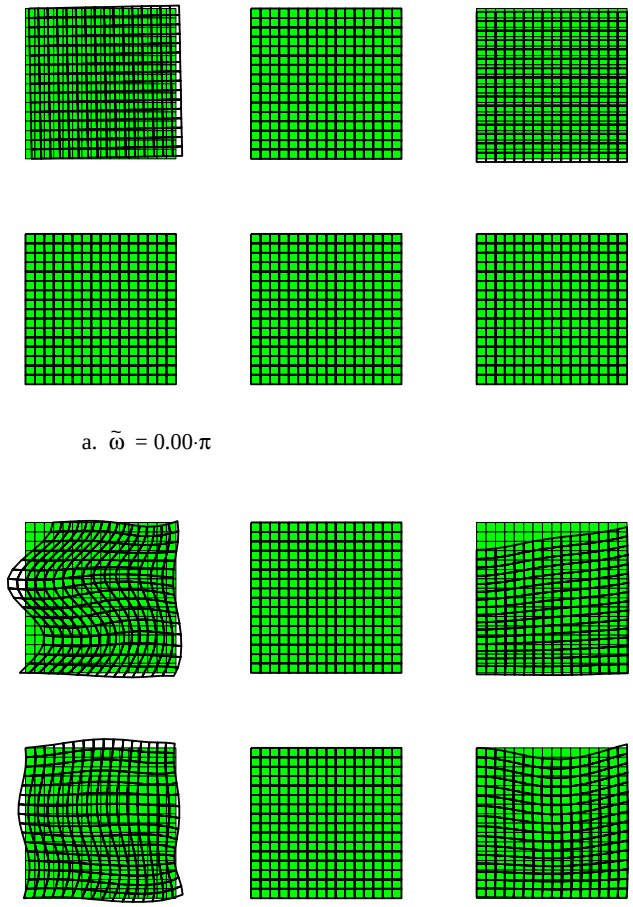

Figure 10. Normalized velocity response shapes $\tilde{v}_x$ at selected frequencies due to application of t_x^{eq}. Case TB without mass-proportional damping.

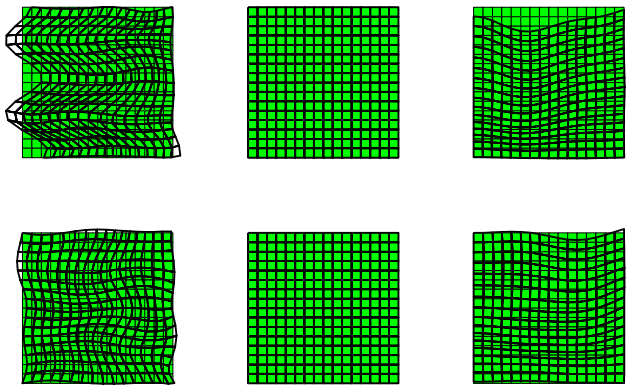

c. $\tilde{\omega} = 4.04 \cdot \pi$

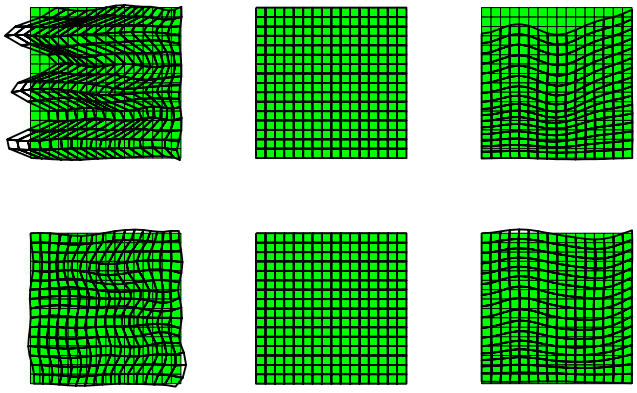

d. $\tilde{\omega} = 5.25 \cdot \pi$

Figure 10. (continued)

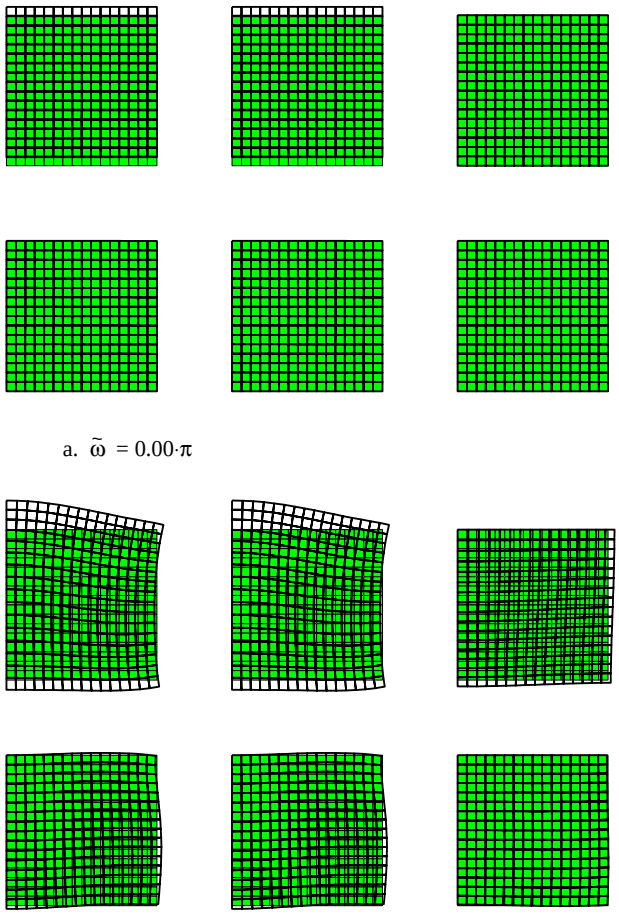

Figure 11. Normalized velocity response shapes $\tilde{v}_z$ at selected frequencies due to application of t_z^{eq}. Case TB without mass-proportional damping.

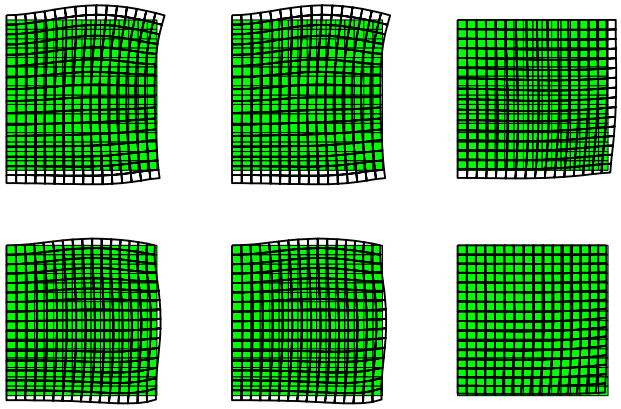

c. $\tilde{\omega} = 1.80 \cdot \pi$

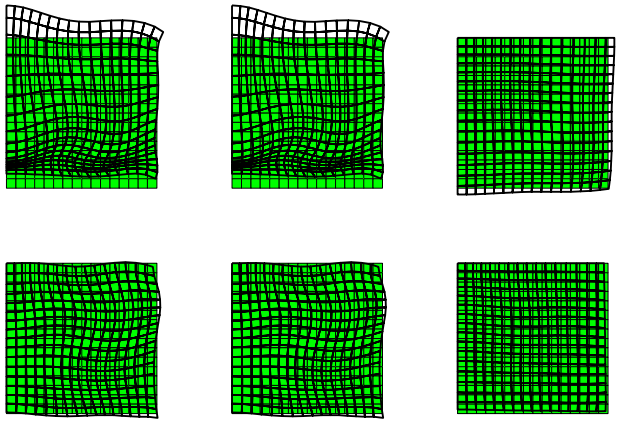

d. $\tilde{\omega} = 3.08 \cdot \pi$

Figure 11. (continued)

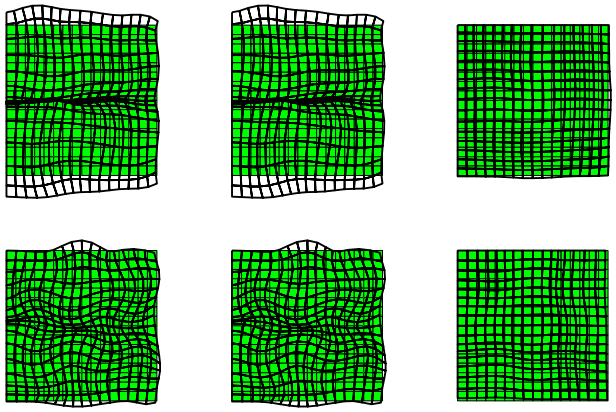

e. $\tilde{\omega} = 4.93 \cdot \pi$

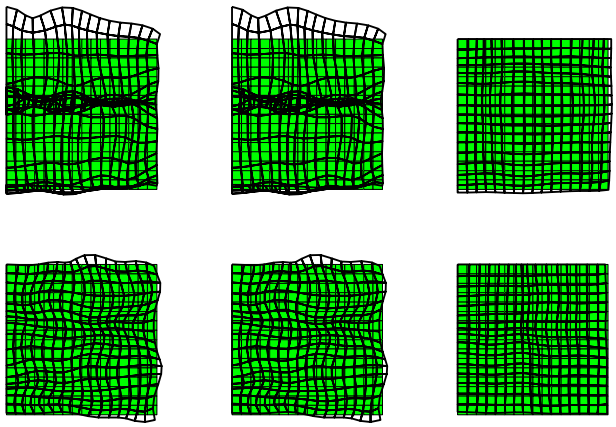

f. $\tilde{\omega} = 5.70 \cdot \pi$

Figure 11. (continued)

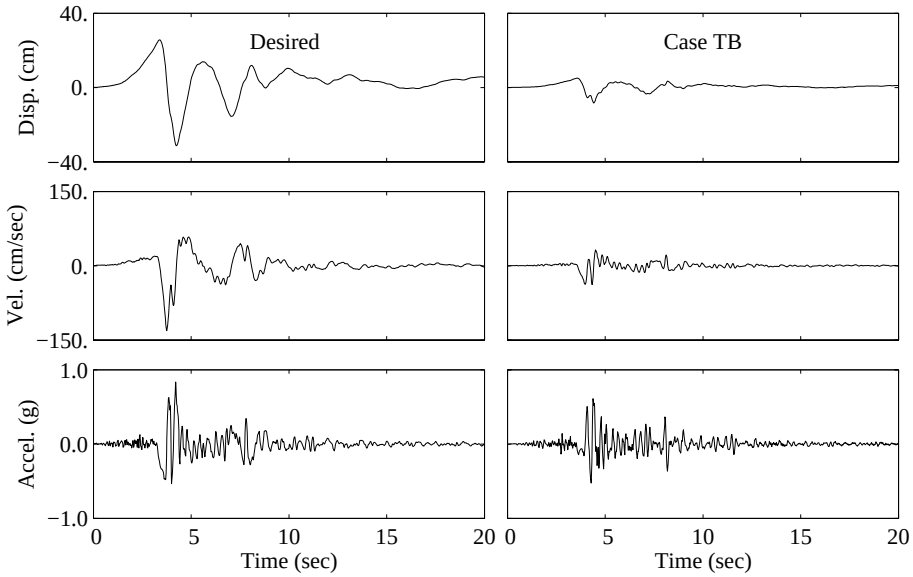

Figure 12. Left: displacement, velocity and acceleration time histories for the ground motions recorded at the Olive View Hospital free-field site during the Northridge earthquake. These are the desired motions for the test block at point C in the x direction. Right: Case TB motions (without mass-proportional damping) are computed by the incident wave method for the test block at point C in the x direction.

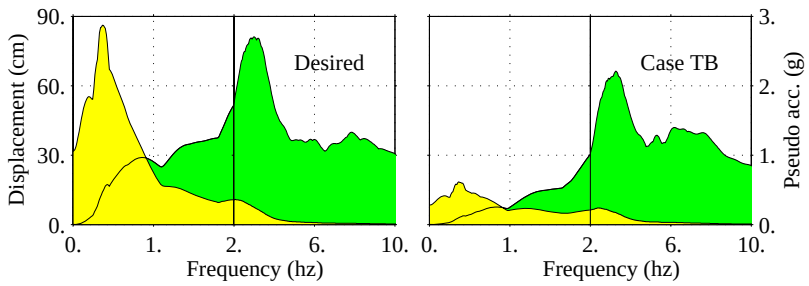

Figure 13. Displacement (light gray) and pseudo acceleration (dark gray) response spectra for the motions shown in Figure 12 (5% damping).

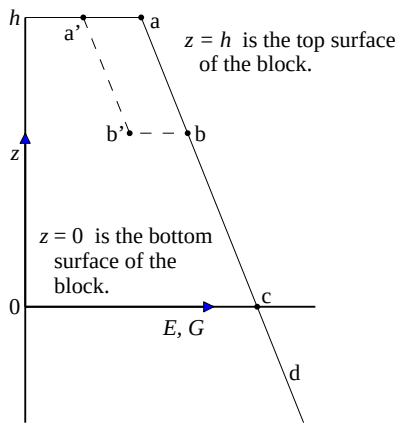

Figure 14. Vertical variation of material properties *E* or *G*. Profile a-b-c-d is from the site where the earthquake ground motion is recorded. Profile a'-b'-b-c-d is from the site of the structure to be analyzed.